Understanding the Effects of Hydrogen Bonding at the Vapor−Water Interface: Vibrational Sum Frequency Spectroscopy of $H_2O/HOD/D_2O$ Mixtures Studied Using Molecular Dynamics Simulations

Dave S. Walker and Geraldine L. Richmond*

Department of Chemistry and Materials Science Institute, University of Oregon, Eugene, Oregon 97403

Received: January 19, 2007; In Final Form: April 4, 2007

Molecular structure and bonding interactions at the vapor−water interface of varying $H_2O/HOD/D_2O$ composition has been calculated using molecular dynamics simulations. From these simulations a surface vibrational sum frequency (VSF) spectrum of the OH stretch region has been generated and compared with experimental VSF results of similar isotopic mixtures. The peak frequency of the uncoupled, solvated OH stretch mode determined from the computational spectrum of the vapor−HOD interface shows excellent agreement with these experimental results. With the addition of H_2O, the calculations performed in this work provide information as to how various OH stretch modes at the vapor−water interface are impacted by the coupling effects that are induced by hydrogen bonding to adjacent OH oscillators. The results of these calculations demonstrate the frequency shifting, spectral broadening, and changes in transition strength exhibited by the OH stretch modes of interfacial water species that occur with increased intermolecular and intramolecular coupling, providing an improved understanding of the different types of water species present at the vapor−water interface that have been difficult to assign in previous VSF experimental studies.

Introduction

Understanding the vibrational spectroscopy of liquid water is a difficult challenge. The impact of the intermolecular and intramolecular couplings caused by hydrogen bonding between water molecules is manifest in its purest form in this simple and most abundant molecular liquid. Because of these coupling effects, excited OH stretch modes in liquid H_2O retain efficient relaxation pathways with their immediate environment, resulting in short lifetimes and large natural linewidths.[1−5] In conjunction with these observations, the correlation between an OH stretch frequency and its intermolecular bond length is poor,[6] making it difficult to assess the impact of hydrogen bonding as a function of OH vibrational frequency. As a result, the vibrational response of water becomes challenging to analyze spectroscopically due to the difficultly in correlating a particular frequency (or even a range of frequencies) of a given OH stretch mode with a particular type of molecular environment.

Water surfaces are ubiquitous; yet only recently have experimental techniques been developed enough to directly probe these interfacial systems. One such technique that has greatly contributed to the understanding of water surfaces is vibrational sum frequency (VSF) spectroscopy. However, the challenge to understand the vibrational response of bulk water carries over to the surface, resulting in a multitude of different experimental interpretations regarding the spectral analysis of the water surface measured using VSF spectroscopy.[7−18] As has been the case for water clusters,[19,20] computational methods have a role to play in unraveling the complexity of water interactions at surfaces. Thus far, computational approaches have used existing molecular models of water to reasonably reproduce the spectral response of interfacial water using classical methods.[21−29] But despite the knowledge available from these and other sophisticated computational approaches,[30,31] much ambiguity still remains regarding the spectral analysis of interfacial water and the complications caused by hydrogen bonding.

A robust method of testing any model while deriving fundamental information about hydrogen bonding in water is to examine mixtures of H_2O, D_2O, and HOD. Such isotopic dilution studies involve replacing H_2O with large concentrations of D_2O with the intent to produce a liquid system that contains only HOD solvated in D_2O. These systems effectively remove much of the coupling effects caused by hydrogen bonding. This approach has been applied in the past with great success toward understanding the structural and dynamical properties of water.[4,6,32−39] Recently, VSF isotopic dilution experiments were performed with the objective of isolating the uncoupled, solvated OH stretch mode of water at the vapor−water interface.[11,12] Spectral parameters of the solvated OH stretch mode of HOD in D_2O were assigned, and a global curve fitting routine was applied to extrapolate this information through the entire range of isotopic mixtures toward the spectral response of pure H_2O. Although the fitting routine produced good agreement with experiments, key parameters (spectral line widths and peak frequencies) were held fixed due to the inability to quantitatively incorporate the impact of intramolecular and intermolecular coupling from adjacent OH stretch oscillators on peak frequencies and spectral line widths. Nevertheless, this experimental approach provides a good starting point for further investigations of interfacial water structure, particularly when examining the effect of adsorbates and ions on the neat vapor−water spectrum.[17]

The studies presented in this paper apply classical molecular dynamics (MD) simulations toward the experimental isotopic dilution measurements recently performed by this laboratory.[12] In particular, these MD simulations produce a computational

* Corresponding author. E-mail: richmond@uoregon.edu. Phone: 541-346-4635. Fax: 541-346-5859.

10.1021/jp070493v CCC: $37.00
Published on Web 05/23/2007

TABLE 1: Isotopic Composition and Names of D_2O, HOD, and H_2O Mixtures

system names	no. of D_2O molecules	no. of HOD molecules	no. of H_2O molecules
d00	0	0	2135
d08	170	873	1089
d33	701	1044	384
d51	1084	873	171
d73	1551	533	43
d81	1726	400	0

VSF spectrum of the vapor−HOD interface. The uncoupled, solvated OH stretch mode is identified with a peak frequency that is in very good agreement with the experimental observations. In addition, the results reported herein identify OH stretch modes by environment and demonstrate how each type of OH stretch mode is impacted by hydrogen bonding throughout the entire isotopic dilution series as the quantity of H_2O is increased toward that of the pure H_2O surface. The overall impact is one of frequency shifting and spectral broadening exhibited by solvated OH stretch modes as a function of H_2O concentration.

Computational Method

The computational approach used to perform MD simulations of these isotopic systems was identical to that applied in recent simulations of the vapor−H_2O interface,[29] so only a brief description will be provided here. Initial bulk liquids were equilibrated for 200 ps in periodic boxes measuring 40 Å in each direction, prior to a 40 Å expansion in the *z* direction producing two vapor−water interfacial systems that related to each other by means of an inversion symmetry operation. Interfacial systems were then equilibrated for 2 ns before data was collected every 50 fs over the course of the next 3 ns. The time step of integration was 1 fs. Molecular geometries were held fixed using the SHAKE algorithm, and the Particle Mesh Ewald technique was applied to handle long-range interactions up to 8 Å. The temperature of the system was 300 K, maintained by weak coupling to a heat bath. The AMBER 7 force field was used to perform the MD simulations of each interfacial system.[40]

Isotopic mixtures of H_2O, HOD, and D_2O were created based on a bulk H_2O composition of 0.997 g/mL and a bulk D_2O composition of 1.1 g/mL. These H_2O, HOD, and D_2O mixtures followed compositions created in recent experimental VSF measurements of isotopic mixtures performed by this laboratory.[12] Table 1 shows the various compositions of H_2O, HOD, and D_2O in each of the isotopic mixtures. Each mixture is described by the volumetric composition of D_2O using the label d%, e.g. d73, which contained 73% D_2O, 25% HOD, and 2% H_2O. Key isotopic mixtures that were studied computationally include d00, correlating to the pure vapor−H_2O system; d81, correlating to the vapor−HOD system with HOD solvated in D_2O; and d73, correlating to the experimental system that contained the largest quantity of D_2O. The POL3 model[40] was used as a basis to describe all molecules, with isotopic dilution represented only by changing the mass of the molecules from 16 (H_2O) to either 17 (HOD) or 18 (D_2O). While quantum mechanical considerations were necessary to completely describe the isotopic effect, the calculation of vibrational frequencies was sufficiently represented in the classical treatment, with OD vibrational frequencies excluded from calculation within the OH stretch frequency range applied in this work (2800−3800 cm^{-1}).

The analysis of the computational approach involved the use of a modified Morita and Hynes (MH) treatment[23] to evaluate the spectral response of water in the frequency domain. The VSF intensity is proportional to the square of the effective macroscopic susceptibility:

$$I_{SFG}\alpha|\chi^{(2)}_{eff}|^2 = |F_{SFG}F_{VIS}F_{IR}(N\langle\beta_{pqr}\rangle + \chi^{(2)}_{NR})|^2 \qquad (1)$$

where β_{pqr} is the molecular hyperpolarizability, defined by

$$\beta_{pqr} \approx \frac{1}{2m\omega}\left(\frac{\partial\alpha_{pq}}{\partial Q}\right)\left(\frac{\partial\mu_r}{\partial Q}\right)\left[\frac{\omega-\omega_{IR}}{(\omega-\omega_{IR})^2+\gamma^2} + \frac{i\gamma}{(\omega-\omega_{IR})^2+\gamma^2}\right] \qquad (2)$$

N is the number of molecules, $\chi^{(2)}_{NR}$ is the nonresonant susceptibility, $F_{SFG}\cdot F_{VIS}\cdot F_{IR}$ is the local field correction, and the derivatives $\partial\mu_r/\partial Q$ and $\partial\alpha_{pq}/\partial Q$ are the infrared transition dipole moment and Raman transition polarizability derivatives, respectively, for an OH normal mode of water with reduced bond mass *m* and frequency ω in the pqr reference frame. The angled brackets $\langle\ \rangle$ represent an orientation average that results in the cancellation of VSF intensity within the bulk liquid due to the random orientation of molecules, and the accumulation of VSF intensity at the liquid interface due to its lack of inversion symmetry. The local field correction, $F_{SFG}\cdot F_{VIS}\cdot F_{IR}$, was defined here as the product of Fresnel coefficients[41] and unit polarization vectors for the incident visible (F_{VIS}) and infrared (F_{IR}) beams along with the detected sum frequency signal (F_{SFG}). The beam angles representative of the unit polarization vectors were based upon the geometry used in the VSF isotopic dilution experiments.[12] The damping term, γ, was treated as an empirical parameter held fixed at 2 cm^{-1}. With the molecular hyperpolarizabilities available via the MH approach, these quantities were projected from the molecular frame into the laboratory frame and binned according to frequency to create the macroscopic susceptibility, $\chi^{(2)}_{ijk}=N\langle\beta_{pqr}\rangle$. In order to compare the calculated macroscopic susceptibility ($\chi^{(2)}_{ijk}$) with the experimental VSF intensity, the nonresonant contribution was treated as an empirical parameter set to −40 au, although this quantity can be determined from ab initio calculations.[24] The calculation of the Fresnel coefficients (used as part of the local field correction) applied frequency-dependent refractive indices of H_2O[42] and D_2O[43] in concentrations applicable toward the corresponding isotopic mixture.

Modifications to the MH technique include a dipole−dipole interaction term for intermolecular OH bonds that exhibit favorable geometric coordination (defined below) and a variable intramolecular coupling constant dependent upon the degree of solvation for a given water molecule.[29] The computational VSF spectrum of the vapor−H_2O interface obtained by means of this modified MH approach was shown to be in very good agreement with experimental measurements in SSP polarization,[29] which probes OH infrared transition dipole moments perpendicular to the interface and is the polarization scheme used to describe the spectral calculations of this work.

Molecules were described as hydrogen-bonded if the intermolecular bond length separating them was less than or equal to 2.5 Å and the corresponding bond angle was less than or equal to 30°. These were described as normal hydrogen bonds and were considered favorable on a geometric basis (thus amenable to dipole−dipole coupling). Molecules that did not satisfy the angle requirement were characterized as broken hydrogen bonds and were considered unfavorable on a geometric basis. (The recognition of broken hydrogen bonds was necessary

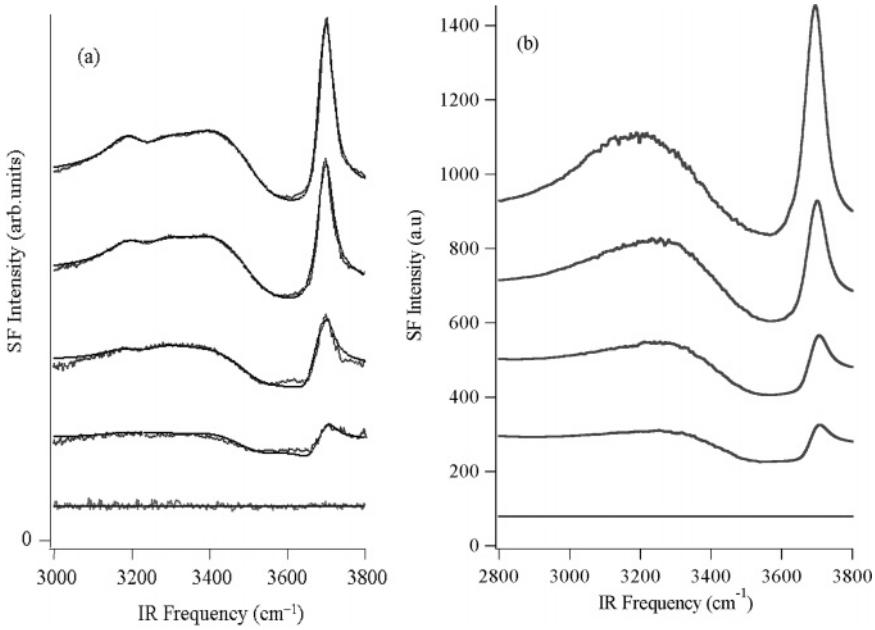

Figure 1. (a) Experimental and (b) computational VSF spectra in SSP polarization of H_2O, HOD, and D_2O mixtures. Spectra have been shifted on the *y*-axis for clarity. Experimental data are taken from refs 12 and 17.

due to their significant contribution to VSF intensity within the OH stretch region of the spectrum.) No distinction between an intermolecular OH bond and an intermolecular OD bond was given when describing the coordination of any given molecule. However, this distinction was fully recognized when applying the coupling and perturbative effects representative of hydrogen bonding. For the dipole−dipole coupling to take place, both oscillators involved must come from OH bonds. (Intermolecular OH−OD coupling was expected to be negligible and was therefore not explicitly treated in this work.) In order for intramolecular coupling to take place, both oscillators involved must be OH bonds. (The spectral response of HOD was treated as a signal emerging from an uncoupled OH oscillator.) Finally, the perturbation caused by hydrogen-bonding that was described in the original MH treatment[23] was only applied when both oscillators involved came from OH bonds, i.e., individual H_2O molecules or adjacent HOD molecules. This perturbative effect modeled the magnitudes of the infrared transition dipole moment and Raman transition polarizability derivatives as a function of OH bond frequency, thus incorporating "transition strength" into the molecular hyperpolarizability.

The naming scheme implemented by Buch[22] was adapted here as in our previous studies of water surfaces.[29] Hydrogen bonds located on hydrogen atoms were identified as "H-bonded" moieties, whereas hydrogen bonds located on oxygen atoms were identified as "O-bonded" moieties. For example, any molecule (H_2O, HOD or D_2O) with tetrahedral coordination was designated as an OOHH-bonded molecule, and any molecule bonded to three adjacent molecules was designated as an OHH-bonded or OOH-bonded molecule. In addition, molecules that exhibited entirely normal hydrogen bonds were given the prefix "*n*-" while molecules that exhibited partial amounts or entire amounts of broken hydrogen bonds where given the prefix "*b*-". Examples of common types of water molecules include molecules with tetrahedral coordination where some or all of their bonds are broken (*b*-OOHH-bonded water) or molecules with one normal hydrogen bond on its oxygen atom and one normal hydrogen bond on its hydrogen atom (*n*-OH-bonded water). Only the four closest hydrogen bonds per molecule were considered for characterization.

The formation of a water surface causes an increase in the population of water molecules that are said to "straddle" the interface.[8,13] These straddling water molecules possess one OH bond with its hydrogen atom pointed into the vapor phase with no hydrogen bonding interactions with adjacent water molecules, and one OH bond with its hydrogen atom pointing toward the water phase that is hydrogen bonded. These two uncoupled bonds have thus been labeled as "free OH" bonds and "donor OH" bonds, respectively. The "free OH mode" is often easy to identify in VSF spectra as a sharp peak at high OH vibrational frequencies. The corresponding "donor OH mode" contributes to the vibrational response of a solvated OH oscillator and as a result is subject to hydrogen bonding. Computationally, these water molecules were treated with the same hydrogen-bonding parameters as were other water molecules and were placed into three categories based upon the degree of bonding on the oxygen atom (H-bonded, OH-bonded, and OOH-bonded molecules). The "total free" OH mode label, without the bonding designation, was used to identify the sum of free OH modes from all three contributors. The donor OH mode also has the possibility of bonding with the three designated categories and will be discussed separately as has been done in previous work.[29] In the computational modeling of these isotopic mixtures, special emphasis was placed on the nature of these straddling water molecules and in particular the free OH mode and the donor OH mode, as these were among the most frequently addressed OH stretch modes within the literature.[9,10,12]

Results and Discussion

Modeling the H_2O/HOD/D_2O Isotopic Dilution Series. Figure 1a,b shows the experimental and computational isotopic dilution series of various H_2O, HOD, and D_2O mixtures in SSP polarization. For both series, the top spectrum corresponds to the neat vapor−H_2O (d00) interface, and the bottom line shape corresponds to the nonresonant susceptibility (which is featureless, indicative of the neat vapor−D_2O interface). Intermittent mixtures of H_2O, HOD, and D_2O lie between in increasing D_2O concentrations from top to bottom. All spectra include the nonresonant contribution and the local field correction. Each spectrum has been shifted on the *y*-axis for clarity with respect

to the nonresonant susceptibility. Figure 1b shows that the computational series reproduces the primary spectral features observed in the experimental spectra including the progressive loss of intensity within the OH stretch region as the quantity of D_2O is increased.

The $H_2O/HOD/D_2O$ isotopic dilution series of water at the vapor−water interface featured in Figure 1a has been studied in great detail in past VSF experiments performed by this laboratory.[12,17] In these studies, a global curve fitting routine has been applied to fit the spectrum of each set of isotopic mixtures with the same set of resonant peak frequencies and widths, allowing only their amplitudes to vary as a function of D_2O concentration. Spectral assignments of water within the OH stretch region have been based on the parameters obtained from these fits, and relied heavily upon the HOD system containing the largest quantity of D_2O (the d73 system, which contains 73% D_2O, 25% HOD, and 2% H_2O). In the d73 system, OH stretch modes are mostly observed from HOD molecules immersed in D_2O, largely removing the intermolecular and intramolecular coupling caused by hydrogen-bonding that complicates the spectral response of H_2O.

To analyze the impact of hydrogen-bonding computationally, and to produce computational results that can be compared to experiment, two systems are of immediate interest for further discussion. The d81 (81% D_2O, 19% HOD) system is of interest as there are no H_2O molecules present, thus maximizing the removal of intermolecular and intramolecular coupling effects and minimizing the impact of hydrogen bonding on the various OH stretch modes that comprise the VSF spectrum. The complete absence of H_2O however is not realistic, so the d73 system is also of interest for analysis. Computational generation of a VSF spectrum for the d73 system enables direct comparison with the experimental result and the spectral parameters obtained from the applied global curve fitting routine. These systems, along with the d00 (vapor−H_2O) interface, will be discussed in greater detail below.

The d00, d81, and d73 Interfaces. Panels a and b of Figure 2 show the experimental and computational resonant spectral responses of the d00 interface in SSP polarization, respectively. Contained within both spectra are two distinct regions: the sharp peak at high frequencies routinely attributed to the free OH mode, and the "solvated OH stretch region", loosely defined in this work as the broad spectral response from OH stretch modes that encompasses several hundred wave numbers at lower frequencies with respect to the free OH peak. The experimental response obtained using global curve fitting contains subtle features within the solvated OH stretch region not observed in the computational result, but the overall agreement between these two approaches is very good. The VSF spectral response of the d00 interface has been studied in great detail both experimentally and computationally,[11,12,29] and so only a brief description will be provided here. Shown in the computational resonant response (Figure 2b) are spectral contributions from the most dominant OH stretch modes. The total free OH mode peaks at approximately 3690 cm^{-1}, in reasonable agreement with the experimentally determined value of 3706 cm^{-1} found from deconvolution of Figure 2a.[12] The *n*-OH-bonded donor OH mode (the donor OH mode from *n*-OH-bonded molecules) peaks at approximately 3310 cm^{-1}.[29] Although there is peak intensity for the *n*-OH-bonded donor OH mode, its spectral contribution spans the entire solvated OH stretch region and is greater than the collective contributions of all other OH stretch modes combined throughout this region in SSP polarization. Additional deconvolution of the peak representing the collective contributions of all other minor OH stretch modes[29] reveals different types of donor OH modes that peak at lower (*n*-OOH-bonded donor OH mode at 3250 cm^{-1}) and higher (H-bonded donor OH mode at 3550 cm^{-1}) frequencies.[9,10] Figure 2c shows the real, imaginary, and nonresonant components of the calculated macroscopic susceptibility of the d00 interface in SSP polarization. The line shapes of these susceptibility components are in good agreement with the susceptibility components obtained from Figure 2a,[12] in addition to other computational measurements of the d00 interface.[23,24]

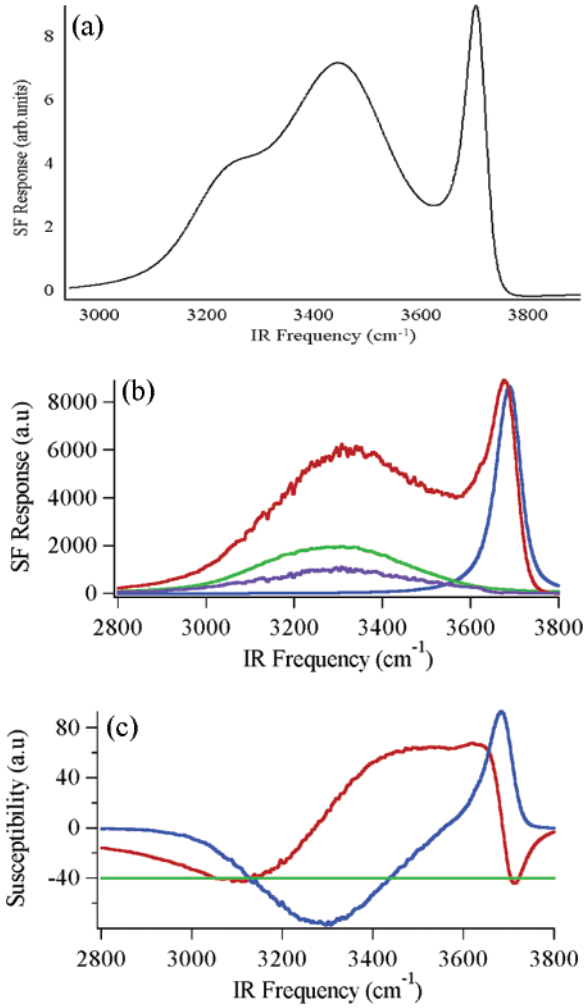

Figure 2. (a) Experimentally determined resonant VSF spectrum of the d00 interface in SSP polarization. (Taken from ref 12.) (b) Computational VSF resonant spectrum of the d00 interface in SSP polarization. Red, total spectrum; blue, total free OH mode; green, *n*-OH-bonded donor OH mode; purple, all other OH stretch modes combined. (c) Real (red), imaginary (blue), and nonresonant (green) components of the macroscopic susceptibility of the d00 interface in SSP polarization.

Figure 3a,b shows representations of the computational resonant spectral response from the d81 interfacial system in SSP polarization. Due to the complete absence of H_2O molecules, only HOD molecules create the spectral response, minimizing the impact of hydrogen bonding in this system. Figure 3a shows the computational VSF spectrum of the d81 interface possesses a large, dominating total free OH peak, followed by a broad peak representative of the solvated OH stretch region. The relative spectral contribution from the total free OH peak (compared to that of the solvated OH stretch region) is much larger in the d81 system compared to the d00 system. Its peak frequency of 3680 cm^{-1} appears to be

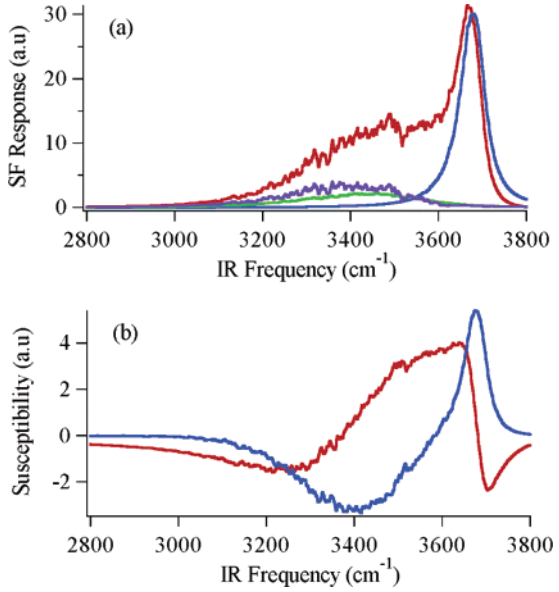

Figure 3. (a) Computational VSF resonant spectrum of the d81 interface in SSP polarization. Red, total spectrum; blue, total free OH mode; green, *n*-OH-bonded donor OH mode; purple, all other OH stretch modes combined. (b) Real (red) and imaginary (blue) components of the macroscopic susceptibility of the d81 interface in SSP polarization.

minimally affected by isotopic dilution, shifted toward lower frequencies by only 10 cm^{-1} with respect to the total free OH peak determined for the d00 system (3690 cm^{-1}). The spectral response of the solvated OH stretch region however is significantly affected by isotopic dilution. Unlike the d00 system where there appears to be two separately peaked spectral regions (the free OH peak and the solvated OH stretch region), the solvated OH stretch region in the d81 system appears as a very broad shoulder on the lower energy side of the free OH peak. Its intensity covers a much narrower spectral range, resulting in negligible response below 3000 cm^{-1}. These observations imply a net blue shift in the solvated OH oscillators of the d81 interface compared to those of the d00 interface, consistent with reduced hydrogen bonding. Spectral deconvolution of the solvated OH stretch region shows the *n*-OH-bonded donor OH mode makes the dominant contribution, comparable to the collective contributions of all other OH stretch modes combined. The peak intensity of the *n*-OH-bonded donor OH mode in this system lies at approximately 3440 cm^{-1}, shifted toward higher frequencies by 130 cm^{-1} with respect to the *n*-OH-bonded donor OH mode measured in the d00 system (3310 cm^{-1}). Figure 3b shows the real and imaginary components of the macroscopic susceptibility for this system. Although there is no H_2O present, these profiles follow the general line shape of the susceptibility profiles observed from the d00 system.

Panels a and b of Figure 4 show the experimental and computational resonant spectral responses of the d73 interfacial system in SSP polarization, respectively. Unlike the d81 computational system, the d73 computational system contains some H_2O molecules and most accurately resembles real systems containing high concentrations of D_2O. Similar to the d00 spectral responses, subtle differences are observed between the fitted experimental result and the computational result within the solvated OH stretch region of the d73 system, but the overall agreement between the two results for the d73 system is also very good. Figure 4b shows the computational VSF spectral response for this system is visually distinguishable from that of the d81 interfacial system (see Figure 3a). The broad peak

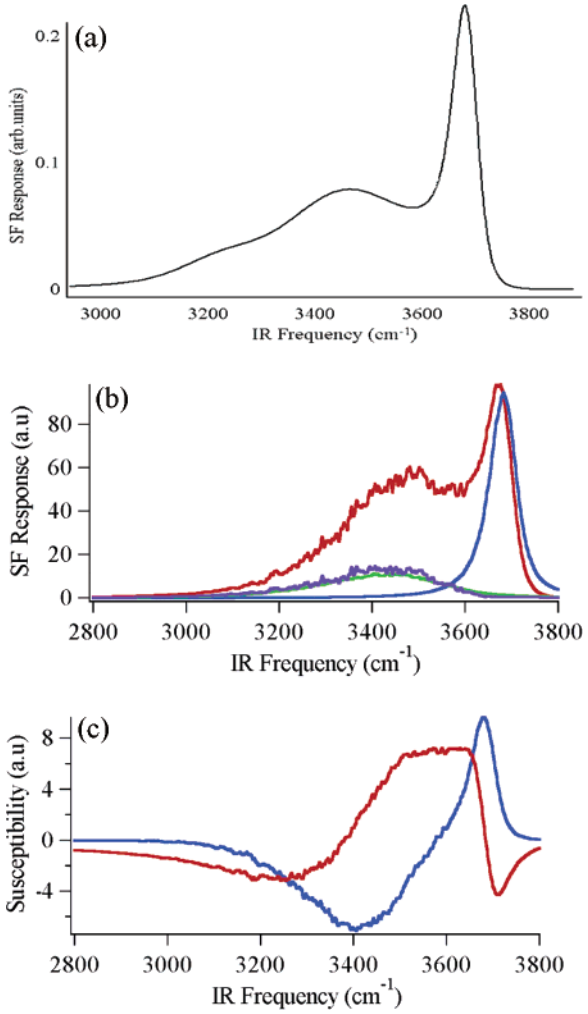

Figure 4. (a) Experimentally determined resonant VSF spectrum of the d73 interface in SSP polarization. (Taken from ref 12.) (b) Computational VSF resonant spectrum of the d73 interface in SSP polarization. Red, total spectrum; blue, total free OH mode; green, *n*-OH-bonded donor OH mode; purple, all other OH stretch modes combined. (b) Real (red) and imaginary (blue) components of the macroscopic susceptibility of the d73 interface in SSP polarization.

representing the solvated OH stretch region shows more intensity relative to the total free OH peak in addition to a somewhat red-shifted spectral distribution. The dominant contributors for this system, as in the d00 and d81 systems, are from *n*-OH-bonded molecules. The *n*-OH-bonded donor OH peak is slightly red-shifted in this system compared to the d81 system (3435 cm^{-1} compared to 3440 cm^{-1}), and the total free OH peak is negligibly shifted to the blue (3682 cm^{-1}). These results compare favorably with the peak frequencies of 3420 cm^{-1} for the uncoupled, solvated OH stretch mode and 3694 cm^{-1} for the free OH mode obtained from deconvolution of Figure 4a.[12] Compared to the d81 system, the slight increase in VSF intensity observed from the solvated OH stretch region is due to both a small red shift in frequency and a small increase in spectral width. Figure 4c shows the real and imaginary components of the macroscopic susceptibility. These susceptibility profiles are in very good agreement with the experimentally determined susceptibility profiles of the equivalent d73 system obtained from Figure 4a.[12]

Unlike VSF intensities, susceptibility profiles contain frequency-dependent phase information that provides insight pertaining to the net orientations of interfacial OH stretch modes that

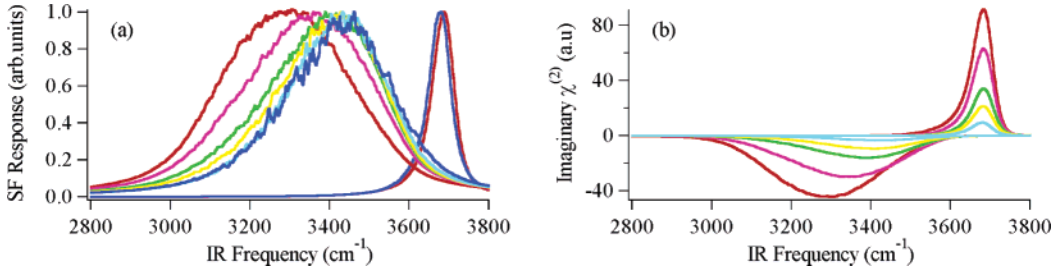

Figure 5. (a) Hydrogen-bonding impact on the VSF responses of the total free OH mode and *n*-OH-bonded donor OH mode. (b) Hydrogen-bonding impact on the imaginary susceptibilities of the total free OH mode and *n*-OH-bonded donor OH mode. Red, d00; purple, d08; green, d33; yellow, d51; light blue, d73; dark blue, d81. Some spectral responses have been removed for clarity.

contribute to the VSF spectral response of water. In this work, the phase is influenced by two components: the symmetries of the OH stretch normal modes in H_2O or HOD, and the orientations of these modes with respect to the water surface. This information is easiest to observe in the imaginary component of the macroscopic susceptibility, where large positive or negative magnitudes represent regions of net constructive interference. The OH normal mode of HOD is totally symmetric only with the lower energy OH normal mode of H_2O, which converges to a symmetric stretch mode when the two OH bonds are in similar environments. In the original MH treatment,[23] the lower energy OH normal mode of H_2O was shown to dominate the solvated OH stretch region, while the higher energy OH normal mode of H_2O dominated the spectral region surrounding the free OH mode. As a result, the consistency of the overall susceptibility profiles generated from the d00, d81, and d73 computational responses suggest that there is no net change in the orientations of OH bonds at the water surface as a function of H_2O concentration. (This argument becomes ambiguous within the spectral region where the higher energy OH normal mode of H_2O is dominant and relies on the assumption that free OH modes from either HOD or H_2O both possess preferential orientations away from the water surface.) In addition, the observation that the available thermal energy at the water surface[12] is sufficiently greater than the difference in energy between a free OH bond and a free OD bond[44] suggests that there is no preferential surface affinity for either OH or OD stretch modes. These observations (no preferential surface affinity or net change in orientation of OH or OD bonds) combine to show the molecular environment of the water surface remains largely constant throughout the entire isotopic dilution series. The dominance of the total free OH peak observed for the d73 and d81 systems is attributed to changes in the transition strength of OH stretch modes rather than changes in molecular environment for these systems of high D_2O concentration compared to systems of high H_2O concentration, i.e., the d00 system. The modeling of this change in transition strength necessitated restricting the perturbative effects of hydrogen bonding found in the original MH treatment[23] toward specific interactions only between adjacent OH bonds.

Hydrogen-Bonding Impact on the Spectral Contributions of OH Stretch Modes. The experimental VSF measurement of the d73 interface is a reliable system to analyze using curve fitting routines due to the removal of hydrogen bonding that complicates the spectral response of the d00 system.[11,12] For a given concentration of H_2O, HOD, and D_2O, a global curve fitting routine was applied toward each set of isotopic mixtures, producing a set of peak parameters with fixed peak frequencies and line widths that were then used to describe the spectral response of the d00 system. Figure 4a,b shows that the computational VSF measurement of the d73 system produced information comparable to the curve fitting results applied toward the d73 experimental spectrum. The constraints applied toward the global curve fitting routines need not be applied within the computational measurement however, and the impact of hydrogen bonding on any given OH stretch mode can be readily calculated for any given isotopic mixture as a function of H_2O concentration.

Previous studies have shown that the major contributor to the intensity in the solvated OH stretch region is the *n*-OH bonded donor mode.[29] Figure 5a,b shows two useful representations that describe the hydrogen-bonding impact on the *n*-OH-bonded donor OH mode and total free OH mode as a function of H_2O concentration. The VSF responses from these modes are normalized to show peak values of unity in Figure 5a, while the actual values of their imaginary susceptibilities are shown in Figure 5b. Both representations reveal the same information, but each representation possesses advantages over the other. VSF responses vary as a function of the square of the number of molecules and need to be normalized due to the vast differences in spectral magnitude for systems high in H_2O concentration compared to systems high in D_2O concentration. This can result in the appearance of very small (or noisy if normalized) responses for OH stretch modes of low signal. Imaginary susceptibilities vary only as a function of the number of molecules and do not require normalization in order to show all concentrations on the same scale. Peak frequencies in imaginary susceptibility values adequately follow their VSF equivalents, thus showing spectral shifts just as well as their corresponding VSF responses. Imaginary susceptibilities also show low signal responses reasonably well, but due to the lack of scaling, broadening effects are not as clear as in the VSF representation.

The spectral responses from the *n*-OH-bonded donor OH mode and the total free OH mode comprise the largest contributions to the VSF spectrum in SSP polarization. Their VSF responses (Figure 5a) sufficiently describe the hydrogen-bonding impact on these modes as a function of H_2O concentration. Figure 5b shows the imaginary susceptibilities of the *n*-OH-bonded donor OH mode and total free OH mode for comparison. Figure 5a shows that as the quantity of H_2O increases, the *n*-OH-bonded donor OH mode undergoes a spectral broadening and a pronounced red shift of about 130 cm^{-1} (from 3440 to 3310 cm^{-1}). The total free OH mode however does not appear to undergo any spectral broadening, and the red shift of approximately 10 cm^{-1} (from 3692 to 3682 cm^{-1}) is barely visible. These results indicate that the *n*-OH-bonded donor OH mode is significantly impacted by hydrogen bonding while the total free OH mode is largely unaffected by hydrogen bonding.

Other types of donor OH mode make minor contributions toward the spectral intensity of the solvated OH stretch region. Figure 6a−d describes the hydrogen-bonding impact on the next lower contributing set of minor donor OH stretch modes as a function of H_2O concentration. The donor OH stretch modes

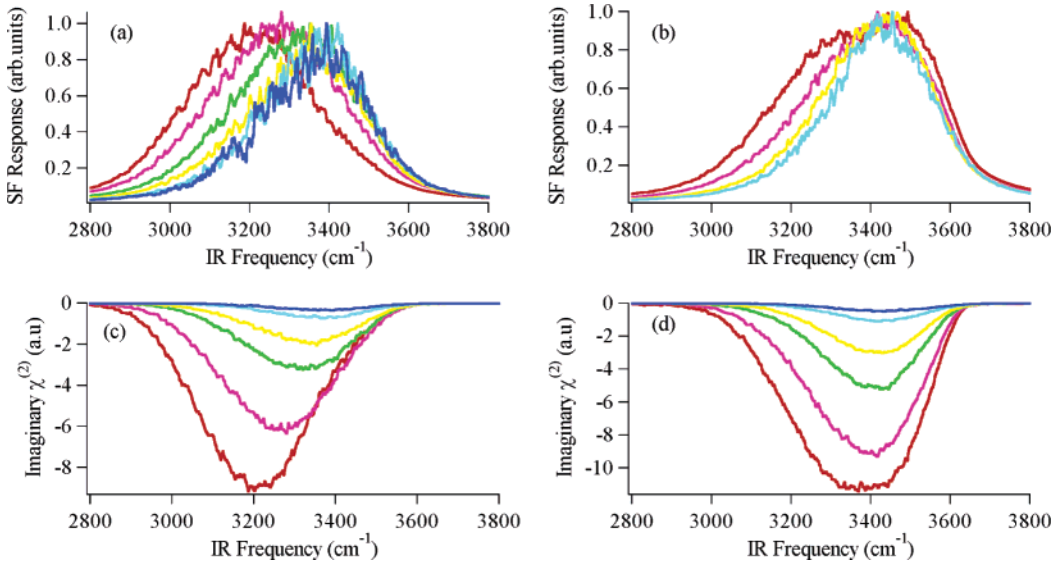

Figure 6. Hydrogen-bonding impacts on (a) the VSF responses of the *n*-OOH-bonded donor OH mode; (b) the VSF responses of the *b*-OOH-bonded donor OH mode; (c) the imaginary susceptibilities of the *n*-OOH-bonded donor OH mode; (d) the imaginary susceptibilities of the *b*-OOH-bonded donor OH mode. Red, d00; purple, d08; green, d33; yellow, d51; light blue, d73; dark blue, d81. Some spectral responses have been removed for clarity.

characterized in these figures are the *n*-OOH-bonded donor OH mode (Figure 6a,c), and the *b*-OOH-bonded donor OH mode (Figure 6b,d). Figure 6a shows the *n*-OOH-bonded donor OH mode undergoes a spectral broadening and red shift in a manner similar to that of the *n*-OH-bonded donor OH mode as the H_2O concentration increases, except over a greater frequency range, indicating that this mode is also significantly impacted by hydrogen bonding. The peak corresponding to the *n*-OOH-bonded donor OH mode shifts from 3390 to 3250 cm^{-1}. Figure 6c shows the hydrogen-bonding impact on the imaginary susceptibilities of the *n*-OOH-bonded donor OH mode as a function of H_2O concentration. In this representation, isotopic mixtures do not require normalization in order to be shown on the same scale. Comparing the imaginary susceptibilities of the *n*-OOH-bonded donor OH mode to the *n*-OH-bonded donor OH mode (Figure 5b) reveals the *n*-OOH-bonded donor OH mode to be approximately four times smaller in its peak magnitude, which approximates to a factor of 16 in peak VSF intensity. The *n*-OH-bonded donor OH mode and *n*-OOH-bonded donor OH mode possess similar bonding geometries with their environment, differing only by a normal hydrogen bond on an acceptor (lone pair) site of oxygen for *n*-OOH-bonded molecules. In this respect a small correlation can be made regarding the degree of the frequency shift and the number of hydrogen bonds per molecule.

Figure 6b,d shows that the *b*-OOH-bonded donor OH mode, also relatively small in spectral response compared to that of the *n*-OH-bonded donor OH mode, is impacted in a very different manner compared to that of the *n*-OOH-bonded donor OH mode. The effect can also be described as a red shift and broadening as the H_2O concentration increases, but unlike these effects displayed by the *n*-OOH-bonded donor OH mode, the spectral broadening dominates over the frequency shift. The frequency shift as a function of H_2O concentration displayed by the *n*-OOH-bonded donor OH mode dominates over the change in width in such a manner that both effects must be included to describe the observed trend, whereas for the *b*-OOH-bonded donor OH mode the observed trend can be described simply by an asymmetric change in the spectral width with a greater change occurring at lower frequencies. As is observed in Figure 6d, the imaginary susceptibilities of the *b*-OOH-bonded donor OH mode possess a slightly larger peak magnitude compared to those of the *n*-OOH-bonded donor OH mode as a function of H_2O concentration, making the spectral contribution of the *b*-OOH-bonded donor OH mode second to the *n*-OH-bonded donor OH mode. This donor OH mode also shows most clearly the broadening effects that occur as a function of H_2O concentration.

Figure 7a−d describes the impact of hydrogen bonding on the *b*-OH-bonded donor OH mode (Figure 7a,c) and the H-bonded donor OH mode (Figure 7b,d) as a function of H_2O concentration. The H-bonded donor OH mode is not separated into *n*-bonded and *b*-bonded moieties due to its small interfacial concentration (0.01 g/mL).[29] These figures show that neither one of these types of donor OH mode are significantly affected by hydrogen bonding, possessing peak intensities at high frequencies throughout the entire concentration range. As is shown in the imaginary susceptibilities of the *b*-OH-bonded donor OH mode (Figure 7c) and the H-bonded donor OH mode (Figure 7d), these types of donor OH mode possess small peak magnitudes and are therefore minor contributors to VSF intensity as a function of H_2O concentration.

Figure 8a−c shows how hydrogen-bonding impacts the imaginary susceptibilities of other minor populations of solvated water molecule as a function of H_2O concentration. These solvated water molecules are *b*-OOHH-bonded water (Figure 8a), b-OHH-bonded water (Figure 8b), and HH-bonded water (Figure 8c). Imaginary susceptibilities are applied exclusively to characterize these OH stretch modes due to their noisy VSF signal at low H_2O concentrations. The general trend observed from these solvated molecules is one of frequency shifting to the red and spectral broadening as the H_2O concentration is increased. These effects appear to be more pronounced based upon the number of hydrogen bond acceptors (hydrogen bonds incident on oxygen atoms) on each of these types of water molecules. The lower energy state values (peak negative values in susceptibility) for *b*-OOHH-bonded water (Figure 8a), *b*-OHH-bonded water (Figure 8b), and HH-bonded water (Figure 8c) approach 3240, 3330, and 3470 cm^{-1}, respectively, in the d00 interfacial system. The assignment of the *b*-OOHH-bonded lower energy value is in good agreement with the peak frequency of 3250 cm^{-1} assigned for water molecules with

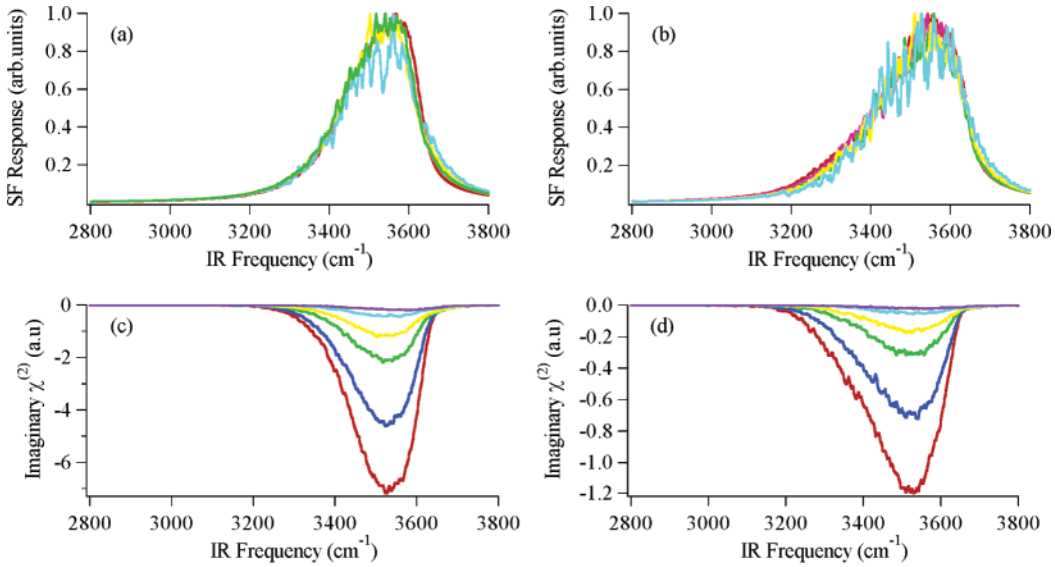

Figure 7. Hydrogen-bonding impacts on (a) the VSF responses of the *b*-OH-bonded donor OH mode; (b) the VSF responses of the H-bonded donor OH mode; (c) the imaginary susceptibilities of the *b*-OH-bonded donor OH mode; (d) the imaginary susceptibilities of the H-bonded donor OH mode. Red, d00; purple, d08; green, d33; yellow, d51; light blue, d73; dark blue, d81. Some spectral responses have been removed for clarity.

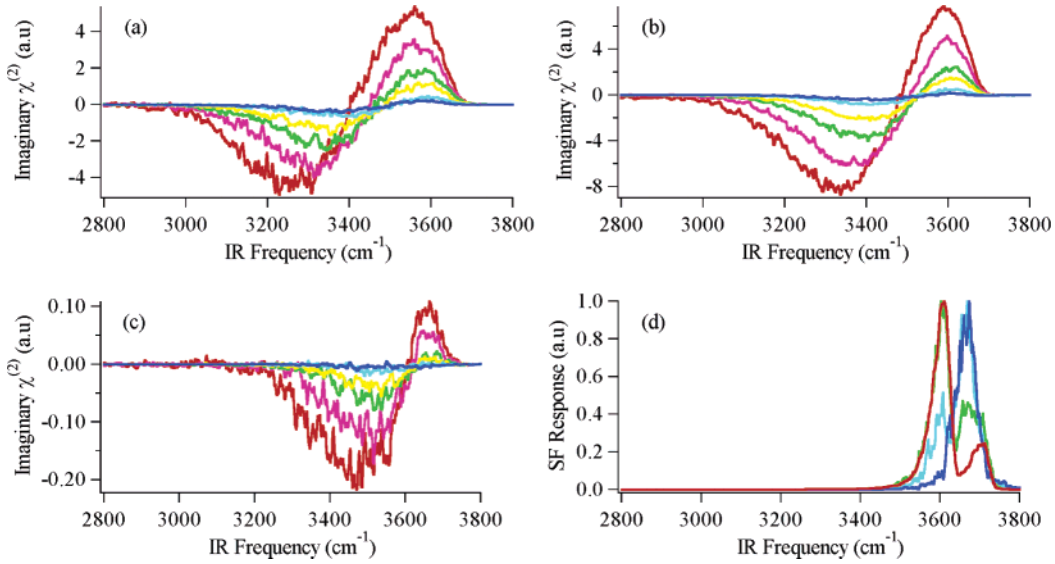

Figure 8. Hydrogen-bonding impacts on (a) the imaginary susceptibilities of *b*-OOHH-bonded water; (b) the imaginary susceptibilities of *b*-OHH-bonded water; (c) the imaginary susceptibilities of HH-bonded water; (d) the VSF responses of OO-bonded water. Red, d00; purple, d08; green, d33; yellow, d51; light blue, d73; dark blue, d81. Some spectral responses have been removed for clarity.

tetrahedral coordination from experimental isotopic dilution experiments.[11,12,17]

Figure 8d describes the hydrogen-bonding impact on the VSF response of OO-bonded water molecules as a function of H_2O concentration. (OO-bonded water molecules comprise the sum of O-bonded and OO-bonded moities due to their low population.) Similar to other OH stretch modes of high frequency, Figure 8d shows that the peak frequencies and widths of OO-bonded water molecules are not affected by hydrogen bonding. The progression of OO-bonded molecules within the isotopic mixtures is unique however from that of other solvated water molecules due to the absence of hydrogen bonds upon the hydrogen atoms of these molecules. An interesting consequence is that for OO-bonded H_2O molecules, the hydrogen atoms are in similar (vapor) environments resulting in clear symmetric and antisymmetric stretch modes. These peaks appear at 3605 and 3710 cm^{-1} for the d00 system. As the quantity of D_2O is increased, the symmetric and antisymmetric stretch modes of H_2O begin to decrease in spectral intensity, and a third peak corresponding to the OH stretch mode of OO-bonded HOD begins to increase in spectral intensity. This third peak appears at 3670 cm^{-1} for the d81 system, which is the system that contains no H_2O molecules. This third peak lies in between the symmetric and antisymmetric OH stretch modes of H_2O, which is to be expected.

It is interesting to note how this computational description of the solvated OH stretch region compares to other descriptions currently within the literature. As mentioned, VSF isotopic dilution experiments were performed in order to isolate the uncoupled, solvated OH stretch mode.[11,12] A global curve fitting routine was then used to extract spectral parameters. These computational results reveal the nature of hydrogen bonding to be more complicated than the description obtained using global curve fitting routines. The spectral response of the d73 system is most adequately described using curve fitting due to the absence of coupling effects felt by individual OH oscillators, and the computational and curve fitting results found for that system are in good agreement. This is most clearly demonstrated

by the identification of the donor OH mode using both approaches, as this OH stretch mode is the largest spectral contributor within the solvated OH stretch region (see Figure 4). In addition, between the computational and curve fitting results, the variance of peak amplitude with OH bond population are in agreement. But the computational result observes an abundance of spectral broadening and spectral shifting as a function of H_2O concentration, variations that are difficult to build into a curve fitting routine for isotopic dilution studies.

Another popular description of the solvated OH stretch region involves the identification of the so-called "ice-like component" (3200 cm^{-1}) and "liquid-like component" (3400 cm^{-1}).[14] To accurately assess the ability of this computational description to confidently elucidate ice-like versus liquid-like components of water would require simulation of the vapor−ice interface.[45] Generally, *n*-bonded water molecules reside closer to 3200 cm^{-1} while *b*-bonded water molecules reside closer to 3400 cm^{-1}. It should be noted however that the spectral response from *n*-OOHH-bonded molecules, the species of water that is most representative of ice, is negligible in these VSF calculations of the vapor−water interface.[29]

In general, these descriptions (tetrahedral and donor OH regions versus ice-like and liquid-like regions) identify two distinct portions of the solvated OH stretch region typically observed in VSF measurements of the vapor−water interface. Regardless of the description, it is important to recognize that solvated OH stretch modes exhibit significant degrees of overlap. For example, complete deconvolution of the vapor−water interface[29] reveals OH-bonded and OOH-bonded molecules make significant spectral contributions at 3200 cm^{-1}, while OH-bonded, OOH-bonded, OHH-bonded, and *b*-OOHH-bonded molecules make significant spectral contributions at 3400 cm^{-1}. This will have a significant impact on time-resolved studies that seek to excite a distinct population of hydrogen-bonded water species by probing a distinct portion of the solvated OH stretch region. Any analysis of the time dependence of the VSF response must take into account these overlapping resonances. However, this complication can be minimized by performing time-resolved experiments on isotopic mixtures of water surfaces with high D_2O concentrations, where the range of environments felt by an OH oscillator are reduced to that of an uncoupled, solvated OH stretch mode.

The overall observation regarding the impact of hydrogen bonding on various types of OH stretch mode in the VSF spectrum is one of spectral broadening, frequency shifting, and changes in transition strength from systems that contain large concentrations of D_2O toward systems that contain large concentrations of H_2O, similar to what is observed in IR and Raman studies of bulk water. These effects are exhibited primarily from solvated molecules, where a correlation can be drawn between the number of hydrogen bond acceptors per molecule and the degree of spectral shifting and broadening for specific types of water molecules. Examples of this are *n*-OOH-bonded donor OH modes versus *n*-OH-bonded donor OH modes versus H-bonded donor OH modes, and *b*-OOHH-bonded water versus *b*-OHH-bonded water versus HH-bonded water. The lack of spectral shifting and broadening exhibited by the total free OH mode and OO-bonded molecules shows that hydrogen bond donors (hydrogen bonds incident upon hydrogen atoms) are necessary to observe any kind of significant impact caused by hydrogen bonding in general. In addition, no overall changes were observed in the molecular environment as a function of D_2O concentration. The spectral dominance of the free OH peak observed in the d73 and d81 interfaces (compared to the d00 interface) demonstrates the reduction of transition strength exhibited by the remaining OH stretch modes that contribute to the spectral response of systems containing high D_2O concentration.

Summary and Conclusions

Spectral calculations of $H_2O/HOD/D_2O$ isotopic mixtures at the vapor−water interface have been performed. The objective of these calculations is to generate a VSF spectrum of the vapor−HOD interface, thus removing the coupling effects induced by hydrogen bonding, which can be directly compared to the VSF spectrum of the vapor−HOD interface measured by this laboratory. With consensus within the experimental and computational VSF community of the spectral assignment of the total free OH mode, an additional objective was to provide a description of the OH stretch modes occupying the solvated portion of the OH stretch region, and in particular the donor OH modes that accompany the total free OH mode. This computational approach leads to a detailed description of how the various donor OH modes and other solvated OH stretch modes are impacted by hydrogen bonding, progressing from systems high in D_2O concentration (where the degree of coupling is small or nonexistent) toward systems high in H_2O concentration. With respect to the vapor−HOD interface, the results of these calculations show that most but not all of the OH stretch modes occupying the solvated OH stretch region undergo a net spectral broadening and red shift as hydrogen bonding is introduced into the system and the vapor−H_2O interface is reached. Also observed as a function of H_2O concentration is a change in the transition strength of OH stretch modes that contribute to the spectral response. This necessitated a restriction by allowing only adjacent OH stretch modes to exhibit the perturbation from hydrogen bonding described in the original MH treatment.[23] Despite the somewhat arbitrary nature of this restriction, the agreement observed between the experimental and computational vapor−HOD spectra is very good.

The computational VSF spectra of the vapor−H_2O (d00) interface and the vapor−HOD (d73) interface shown in this work are in good agreement with the equivalent experimental systems recently obtained by this laboratory.[11,12] These computational results show a negligibly small spectral shift in the total free OH mode as a function of isotopic concentration, and identifies the *n*-OH-bonded donor OH mode as the dominant contributing donor OH species with a peak spectral intensity of 3435 cm^{-1} for systems high in D_2O concentration, in agreement with experimental observations. This *n*-OH-bonded donor OH mode continues to dominate the VSF spectrum with increased H_2O concentration. These computational results also show the effect of hydrogen bonding on other minor species, the *n*-OOH-bonded donor OH mode and H-bonded donor OH mode that have been identified in VSF experiments performed by other laboratories.[9,10] Detailed information about their relative populations and the impact of hydrogen bonding on each of these smaller populations of donor OH modes as a function of H_2O concentration is given.

In the d00 and d73 interfacial systems, subtle differences were observed within the solvated OH stretch region between the experimental fits and the computational results. This difference was more pronounced for the d00 system than for the d73 system. Recent developments in ultrafast vibrational spectroscopy have provided useful information regarding the role of the 2δ bending overtone of water, which appears at approximately 3200 cm^{-1} within the OH stretch region of liquid

H_2O.[1,4] In addition, collective OH stretch motions of H_2O recently discussed in the theoretical work involving ice clusters[46] and water surfaces[22] impact the lower frequency region of the OH stretch spectrum of H_2O. These factors would have a greater effect on water surfaces of high H_2O concentration compared to those of high D_2O concentration. Their absence from this computational treatment presents a viable explanation for the subtle differences observed between the experimental and computational spectral responses within the solvated OH stretch region of the d00 and d73 interfaces.

As such an important interfacial system, the surface of liquid H_2O is routinely the starting point for VSF investigations of a variety of vapor−liquid, liquid−liquid, and solid−liquid interfacial systems.[13,14] Understanding the details behind the spectral response of liquid H_2O has historically been a difficult process due to the strong connectivity between H_2O molecules, generally referred to as hydrogen bonding, that causes unusually fast relaxation times and correspondingly large degrees of spectral broadening within the OH stretch region. These MD simulations provide a detailed description of the OH stretch modes present at the water surface, but also emphasizes the need to start with simpler systems when it comes to understanding the OH spectral response of water on both an experimental and computational basis. The correlations between the spectral response of the vapor−HOD interface and the spectral response of the vapor−H_2O interface are shown to be rather complicated, but with the removal of hydrogen bonding, the details of the vapor−HOD interface are at least shown to be simpler than that of vapor−H_2O and perhaps a better starting point for understanding the water surface, on both a computational and experimental basis.

Acknowledgment. The authors would like to thank the National Science Foundation (CHE 0243856) and the Office of Naval Research for supporting this study. We would also like to acknowledge the helpful assistance of Prof. Dennis Hore and Prof. Fred Moore in preparation of this work and manuscript.

References and Notes

(1) Linder, J.; Vohringer, P.; Pshenichnikov, M. S.; Cringus, D.; Wiersma, D. A.; Mostovoy, M. *Chem. Phys. Lett.* **2006**, *421*, 329.
(2) Liu, P.; Harder, E.; Berne, B. J. *J. Phys. Chem. B* **2005**, *109*, 2949.
(3) Raiteri, P.; Laio, A.; Parrinello, M. *Phys. Rev. Lett.* **2004**, *93*, 087801.
(4) Wang, Z.; Pakoulev, A.; Pang, Y.; Dlott, D. D. *J. Phys. Chem. A* **2004**, *108*, 9054.
(5) Huse, N.; Ashihara, S.; Nibbering, E. T. J.; Elsaesser, T. *Chem. Phys. Lett.* **2005**, *404*, 389.
(6) Moller, K. B.; Rey, R.; Hynes, J. T. *J. Phys. Chem. A* **2004**, *108*, 1275.
(7) Mucha, M.; Frigato, T.; Levering, L. M.; Allen, H.; Tobias, D. J.; Dang, L. X.; Jungwirth, P. *J. Phys. Chem. B* **2005**, *109*, 7617.
(8) Brown, M. G.; Raymond, E. A.; Allen, H.; Scatena, L. F.; Richmond, G. L. *J. Phys. Chem. A* **2000**, *104*, 10220.
(9) Gan, W.; Wu, D.; Zhang, Z.; Feng, R.; Wang, H. F. *J. Chem. Phys.* **2006**, *124*, 114705.
(10) Liu, D.; Ma, G.; Levering, L. M.; Allen, H. *J. Phys. Chem. B* **2004**, *108*, 2252.
(11) Raymond, E. A.; Tarbuck, T. L.; Richmond, G. L. *J. Phys. Chem. B* **2002**, *106*, 2817−2820.
(12) Raymond, E. A.; Tarbuck, T. L.; Brown, M. G.; Richmond, G. L. *J. Phys. Chem. B* **2003**, *107*, 546−556.
(13) Richmond, G. L. *Chem. Rev.* **2002**, *102*, 2693.
(14) Shen, Y. R.; Ostroverkhov, V. *Chem. Rev.* **2006**, *106*, 1140.
(15) Shultz, M. J.; Baldelli, S.; Schnitzer, C.; Simonelli, D. *J. Phys. Chem. B* **2002**, *106*, 5313.
(16) Superfine, R.; Du, Q.; Freysz, E.; Shen, Y. R. *Phys. Rev. Lett.* **1993**, *70*, 2313.
(17) Tarbuck, T. L.; Ota, S. T.; Richmond, G. L. *J. Am. Chem. Soc.* **2006**, *128*, 14519.
(18) Du, Q.; Freysz, E.; Shen, Y. R. *Science* **1994**, *264*, 826.
(19) Sadlej, J.; Buch, V.; Kazimirski, J. K.; Buck, U. *J. Phys. Chem. A* **1999**, *103*, 4933.
(20) Devlin, J. P.; Joyce, C.; Buch, V. *J. Phys. Chem. A* **2000**, *104*, 1974.
(21) Benjamin, I. *Phys. Rev. Lett.* **1994**, *73*, 2083.
(22) Buch, V. *J. Phys. Chem. B* **2005**, *109*, 17771.
(23) Morita, A.; Hynes, J. T. *Chem. Phys.* **2000**, *258*, 371.
(24) Morita, A.; Hynes, J. T. *J. Phys. Chem. B* **2002**, *106*, 673.
(25) Morita, A. *J. Phys. Chem. B* **2006**, *110*, 3158.
(26) Perry, A.; Ahlborn, H.; Space, B. *J. Chem. Phys.* **2003**, *118*, 8411.
(27) Perry, A.; Neipert, C.; Kasprzyk, C. R.; Green, T.; Space, B. *J. Chem. Phys.* **2005**, *123*, 11.
(28) Perry, A.; Neipert, C.; Ridley, C.; Space, B. *Phys. Rev. E* **2005**, *71*, 4.
(29) Walker, D. S.; Hore, D. K.; Richmond, G. L. *J. Phys. Chem. B* **2006**, *110*, 20451.
(30) Kuo, W.; Mundy, C. J.; Eggimann, B. L.; McGrath, M. J.; Siepmann, J. I.; Chen, B.; Vieceli, J.; Tobias, D. J. *J. Phys. Chem. B* **2006**, *110*, 3738.
(31) Feng, I.; Kuo, W.; Mundy, C. J. *Science* **2004**, *303*, 658.
(32) Asbury, J. B.; Steinel, T.; Kwak, K.; Corcelli, S. A.; Lawrence, C. P.; Skinner, J. L.; Fayer, M. D. *J. Chem. Phys.* **2004**, *121*, 12431.
(33) Bakker, H. J.; Woutersen, S.; Nienhuys, H. K. *Chem. Phys.* **2000**, *258*, 233.
(34) Chen, B.; Ivanov, I.; Klein, M.; Parrinello, M. *Phys. Rev. Lett.* **2003**, *91*, 215503.
(35) Corcelli, S. A.; Lawrence, C. P.; Skinner, J. L. *J. Chem. Phys.* **2004**, *120*, 8107.
(36) Fecko, C.; Loparo, J. J.; Roberts, S. T.; Tokmakoff, A. *J. Chem. Phys.* **2005**, *122*, 054506.
(37) Lawrence, C. P.; Skinner, J. L. *J. Chem. Phys.* **2003**, *118*, 264.
(38) Lawrence, C. P.; Skinner, J. L. *Chem. Phys. Lett.* **2003**, *369*, 472.
(39) Rey, R.; Hynes, J. T. *J. Chem. Phys.* **1996**, *104*, 2356.
(40) Case, D. A.; Pearlman, D. A.; Caldwell, J. W.; Cheatham III, T. E.; Wang, J.; Ross, W. S.; Simmerling, C. L.; Darden, T. A.; Merz, K. M.; Stanton, R. V.; Cheng, A. L.; Vincent, J. J.; Crowley, M.; Tsui, V.; Gohlke, H.; Radmer, R. J.; Duan, Y.; Pitera, J.; Massova, I.; Seibel, G. L.; Singh, U. C.; Weiner, P. K.; Kollman, P. A. *AMBER 7*; University of California: San Francisco 2002.
(41) Lobau, J.; Wolfrum, K. *J. Opt. Soc. Am. B* **1997**, *14*, 2505.
(42) Bertie, J. E.; Lan, Z. *App. Spectrosc.* **1996**, *50*, 1047.
(43) Bertie, J. E.; Ahmed, M. K.; Eysel, H. H. *J. Phys. Chem.* **1989**, *93*, 2210.
(44) Devlin, J. P. *J. Chem. Phys.* **2000**, *112*, 5527.
(45) Wei, X.; Miranda, P. B.; Zhang, C.; Shen, Y. R. *Phys. Rev. B* **2002**, *66*, 085401.
(46) Buch, V.; Devlin, J. P. *J. Chem. Phys.* **1999**, *110*, 3437.